Particle dynamics in a symmetrically driven underdamped inhomogeneous periodic potential system

D. Kharkongor,[1] W. L. Reenbohn,[2] and Mangal C. Mahato[1,*]

[1]*Department of Physics, North-Eastern Hill University, Shillong-793022, India*
[2]*Department of Physics, National Institute of Technology Meghalaya, Shillong-793003, India*

We numerically solve the underdamped Langevin equation to obtain the trajectories of a particle in a sinusoidal potential driven by a temporally sinusoidal force in a medium with coefficient of friction periodic in space as the potential but with a phase difference. With the appropriate choice of system parameters, like the mean friction coefficient and the period of the applied field, only two kinds of periodic trajectories are obtained for all possible initial conditions at low noise strengths: one with a large amplitude and a large phase lag with respect to the applied field and the other with a small amplitude and a small phase lag. Thus, the periodic potential system is effectively mapped dynamically into a bistable system. Though the directional asymmetry, brought about only by the frictional inhomogeneity, is weak we find both the phenomena of stochastic resonance, with ready explanation in terms of the two dynamical states of trajectories, and ratchet effect simultaneously in the same parameter space. We analyze the results in detail attempting to find plausible explanations for each.

I. INTRODUCTION

In this work we explore the possibility of whether an inhomogeneous underdamped sinusoidal potential [1] system can be an appropriate candidate for obtaining ratchet current [2–8] while simultaneously exhibiting stochastic resonance [9–14]. In other words, whether in an inhomogeneous system one can obtain an optimally improved response to a sub-threshold external field as the temperature is raised (stochastic resonance) in addition to exhibiting net asymmetric transport (ratchet effect) in a sinusoidal potential without the application of an external bias or with the application of an external field that, on its own, on the average, adds up to equal impulse in opposing directions.

Stochastic resonance was shown earlier to occur in sinusoidal potentials [15–17] contrary to its absence having been stressed previously [18]. It follows from the realization that when driven at a suitably large frequency, an underdamped particle moving in the sinusoidal potential shows two kinds of response trajectories, one with a large amplitude [(LA) and also large phase lag with respect to the drive] and the other with a small amplitude [(SA) and small phase lag]. These solutions are quite robust and have the status of dynamical states. The characteristics that fully establish the trajectories as dynamical states are discussed in detail in Ref. [15]. The motion (trajectory) of the particle can be in either of these two states at any given instant of time. This is especially clearly observable at lower temperatures before the occurrence of stochastic resonance. Therefore, dynamically the system can be considered as bistable. The transition between these dynamical states, as the temperature is raised, can provide an explanation for the occurrence of stochastic resonance in periodic potentials. As far as the phenomenon of stochastic resonance is concerned, the sinusoidal potential thus recedes into oblivion and the problem is recast into one in a bistable system. This is important, for it is in the bistable systems that stochastic resonance is commonly observed.

The two dynamical states and the transitions between them refer mostly to trajectories about the minimum within a period of the periodic potential. However, the statement "stochastic resonance in a periodic potential" is meaningful only if the motion includes not only inter- (dynamical) state transitions present but also movements between various wells (periods) of the potential. In other words, the "bistability" must be maintained at whichever period of the sinusoidal potential the particle happens to occupy as time progresses so the full sinusoidal potential, and not just one period of it, is found to be accessed. Given the criterion to be satisfied, the occurrence of stochastic resonance is discussed only in terms of the two dynamical states and any reference to the sinusoidal potential is conveniently kept silent. However, sometimes, the reference to the interwell transitions has to be alluded to in order to check the credibility of the claim of occurrence of stochastic resonance in periodic potentials. In fact, well before stochastic resonance occurs, numerous interwell transitions take place. As the temperature becomes much larger than the temperature at which stochastic resonance occurs, the transitions become so frequent that the two dynamical states become hardly discernible with separate identity, for the intervals of existence of the two states become too short (could even be less than a period).

By an inhomogeneous system, we mean, in the present work, a system with a nonuniform (space-dependent) friction coefficient. It has been theoretically shown earlier that an overdamped particle experiences a net effective driving force when subjected to a drift in a sinusoidal potential and also a sinusoidally modulated space-dependent diffusion, with the same period as the potential [19]. However, diffusion coefficient D depends on both the temperature T and the friction coefficient γ: $D \sim \frac{T}{\gamma}$. The effect of temperature variation is considered dominant as it determines the local stability of states [19,20]. It has been shown analytically that in an underdamped periodic potential a similarly periodic variation of temperature but with a phase difference leads to ratchet current [21]. This remarkable result was also supported numerically in a related work [22]. The effect of friction coefficient variation is weak and, unlike temperature variation,

a mere similar periodic variation of friction coefficient is not expected to yield ratchet current; to yield ratchet current, in this case, one needs to apply, in addition, a zero-mean external forcing [23].

The ratchet effect has been studied in nonuniform friction periodic potential systems earlier, too, but mostly in the overdamped limit [24], unlike in the present case of underdamped systems. Also, the period of the drive taken earlier used to be very large, typically of the order of mean first passage time across a potential barrier. In these circumstances, stochastic resonance in the periodic potential systems was not found to occur and hence there was no question of exploring whether both the effects occur simultaneously in the same parameter space.

As stated earlier, in addition to the ratchet effect discussed above, the present work endeavours to observe stochastic resonance (SR) simultaneously in the same parameter space. Though the present work is not experimental, it is not hard to think of an easy-to-visualize experimental situation illustrating the present case. Consider a series of nodes and antinodes, created by a stationary pressure wave, representing sites of alternate low and high density of the medium. A particle, therefore, while moving along longitudinally, experiences a periodic variation of friction. In addition, if the particle is charged and an alternating electric potential field, of same wavelength as the pressure wave but with a phase difference, is created the particle will experience a spatially periodic force field. The application of a temporally sinusoidal external electric field completes the illustrative experimental situation to describe the problem at hand and allows the following questions to be asked. Is it possible to obtain a net (ratchet) current? If a thermal noise is added and increased gradually, either through the external field or the system itself, then will the response of a host of particles to the external field be sharper or more smeared? In other words, does the quality of response, as conventionally measured by the (output) signal-to- (input) noise ratio, improve as the noise level is gradually increased? If the response shows a peak (stochastic resonance) at an intermediate temperature (noise strength), then does the net particle current also exhibit a maximum, simultaneously [25]? These are some of the questions that will be attempted to be clarified in a model system.

These questions together have already been discussed earlier, however, in a uniform friction medium and subjected to a biharmonic external field [26], $F(t) = F_0[A\cos(\omega t) + B\cos(2\omega t)]$. In the present work, the potential is considered sinusoidal $V(x) = -V_0 \sin(x)$ and an external field of $F(t) = F_0 \cos(\omega t)$. The asymmetry in the system is introduced via the phase-shifted nonuniform friction $\gamma(x) = \gamma_0[1 - \lambda \sin(x + \theta)]$, with $0 \leqslant \lambda \leqslant 1$. In the case of temperature inhomogeneity, similar in form to the frictional inhomogeneity considered here, it has been shown earlier [21,22] that the ratchet current $\overline{v}$ depends on the phase difference θ between the potential function and the temperature function as $\overline{v} \sim \sin(\theta)$. Thus, understandably, the ratchet current is maximum when the asymmetry is maximum, namely for $\theta = \frac{\pi}{2}$, and the same should be true in the present case of frictional inhomogeneity as well.

Interestingly, for $\theta = \frac{\pi}{2}$, the inhomogeneous friction yields particle trajectories (and stochastic resonance) qualitatively

similar to the uniform friction case in response to the same sinusoidal external field (see Sec. III). However, the inhomogeneous friction, in addition, helps in obtaining a net (ratchet) current. Since, in both the cases, the trajectories show same periodicity as the external field, the particle spends almost the same time in the small and large friction regions which lie, respectively, on either side of the potential minimum. The present situation therefore differs considerably from the adiabatic drive case wherein the particle is likely to spend unequal durations in the two friction regions. Hence the reason put forth for the explanation of occurrence of ratchet current in the adiabatic limit will not hold in the finite frequency drive case [23]. A closer statistical analysis of the parts of trajectories in the two separate regions, however, hints at why the net (asymmetric) particle current should be expected.

The turning points of the trajectories on either side of potential minimum ($x = \frac{\pi}{2}$) show interesting distributions. At very low temperatures, ($T < 0.005$), the mean distance of turning points, dx_r (in the high friction side of the potential peak) and dx_l (in the low friction side) from $x = \frac{\pi}{2}$ and their standard deviations, Δx_r and Δx_l, about the mean values on both sides are same, showing that the motion remains symmetrical on both directions, for all $\tau = \frac{2\pi}{\omega}$. However, as T is gradually increased, the differences show up for $\lambda \neq 0$ and $\theta = \frac{\pi}{2}$. For $\tau = 7.0$ and at low temperatures, only large-amplitude trajectories appear (see Sec. III, Fig. 9). In this case, one obtains $dx_l > dx_r$ and $\Delta x_l > \Delta x_r$ up to a reasonably large temperature. Moreover, for $\tau = 13.0$ and at low temperatures, only small-amplitude trajectories appear in which case one finds $dx_r > dx_l$ and $\Delta x_l \sim \Delta x_r$. However, since interwell transitions and hence ratchet current are dominantly determined by the large amplitude trajectories, there is a higher likelihood of right-to-left net transport than the other way around. Of course, differences of dx_l and dx_r, etc., are very small (less than 1%) and the interwell transitions are thus decided by the rare large-amplitude events.

In Sec. II, the model system of our study will be described. In Sec. III the numerical results based on our investigations will be presented in detail and in Sec. IV our results will be discussed and summarized.

II. THE MODEL

We consider the motion of an ensemble of underdamped noninteracting Brownian particles each of mass m in a periodic potential $V(x) = -V_0 \sin(kx)$. The medium in which the particle moves is taken to be inhomogeneous in the sense that it offers a spatially varying friction with coefficient

$$\gamma(x) = \gamma_0[1 - \lambda \sin(kx + \theta)] \qquad (2.1)$$

that leads/lags the potential by a phase difference θ. This choice of friction coefficient breaks the right-left spatial symmetry of the system. Here, λ is the inhomogeneity parameter, with $0 \leqslant \lambda \leqslant 1$ and hence $\gamma_0(1 - \lambda) \leqslant \gamma(x) \leqslant \gamma_0(1 + \lambda)$.

In addition, the potential is rocked by a subthreshold periodic time-dependent forcing $F(t) = F_0 \cos(\omega t)$, with $\omega = 2\pi/\tau$ as the rocking frequency and τ as the rocking period. The equation of motion of the particle subjected to a thermal Gaussian white noise $\xi(t)$ at temperature T is given by the

Langevin equation [27,28]

$$m\frac{d^2x}{dt^2} = -\gamma(x)\frac{dx}{dt} - \frac{\partial V(x)}{\partial x} + F(t) + \sqrt{\gamma(x)T}\xi(t) \quad (2.2)$$

with

$$\langle \xi(t) \rangle = 0, \langle \xi(t)\xi(t') \rangle = 2\delta(t - t'). \quad (2.3)$$

Here, and throughout the text, $\langle .. \rangle$ correspond to ensemble averages.

For simplicity and convenience, the equation is transformed into dimensionless units [29] by setting $m = 1$, $V_0 = 1$, $k = 1$, with reduced variables denoted again by the same symbols. Thus, the Langevin equation takes the form

$$\frac{d^2x}{dt^2} = -\gamma(x)\frac{dx}{dt} - \frac{\partial V(x)}{\partial x} + F(t) + \sqrt{\gamma(x)T}\xi(t), \quad (2.4)$$

where the potential is reduced to $V(x) = -\sin(x)$ and

$$\gamma(x) = \gamma_0[1 - \lambda \sin(x + \theta)]. \quad (2.5)$$

Equation (2.4) is numerically solved (i.e., integrated using Ito definition) to obtain the trajectories $x(t)$ of the particle for various initial conditions [30–32]. For initial positions $x(t = 0)$ the period $-\frac{\pi}{2} < x \leqslant \frac{3\pi}{2}$ is divided uniformly into either $n = 100$ or $n = 200$ parts (and hence n initial positions) and the initial velocity $v(t = 0)$ is set equal to zero throughout in the following.

III. NUMERICAL RESULTS

For each trajectory, corresponding to one initial position $x(0)$, the work done by the field $F(t)$ on the system, or the input energy, is calculated as [33]

$$W(0, N\tau) = \int_0^{N\tau} \frac{\partial U(x(t), t)}{\partial t} dt, \quad (3.1)$$

where N is a large integer denoting the number of periods taken to reach the final point of the trajectory. The effective potential U is given by

$$U(x(t), t) = V[x(t)] - x(t)F(t). \quad (3.2)$$

The mean input energy per period, for the particular trajectory, is therefore given by

$$\overline{W} = \frac{1}{N}W(0, N\tau). \quad (3.3)$$

For the deterministic case ($T \to 0$, for example, $T = 10^{-6}$) and also at low temperatures [low noise strengths, typically less than about 10% of the largest potential barrier corresponding to $F(t)$], the trajectories $x(t)$ appear to be periodic and similar in nature to that of $F(t)$. Since $V(x)$ is not explicitly dependent on time, all of the contribution to $W(0, N\tau)$ comes from the second term in U, Eq. (3.2), because of the phase difference between $F(t)$ and $x(t)$. The nonzero phase difference also implies hysteresis $\overline{x(F)}$, whose area is a measure of energy dissipation per period by the system. A typical mean hysteresis loop is shown in Fig. 1. Not surprisingly, therefore, it turns out that the corresponding mean hysteresis loop area $\overline{A}$ is the same as $\overline{W}$. The overall mean input energy per period, $\langle \overline{W} \rangle$, is calculated as an (ensemble) average over all the n trajectories (corresponding to all the initial positions considered). Again, we find that $\langle \overline{A} \rangle = \langle \overline{W} \rangle$. Similarly, the mean velocity $\overline{v}$, over
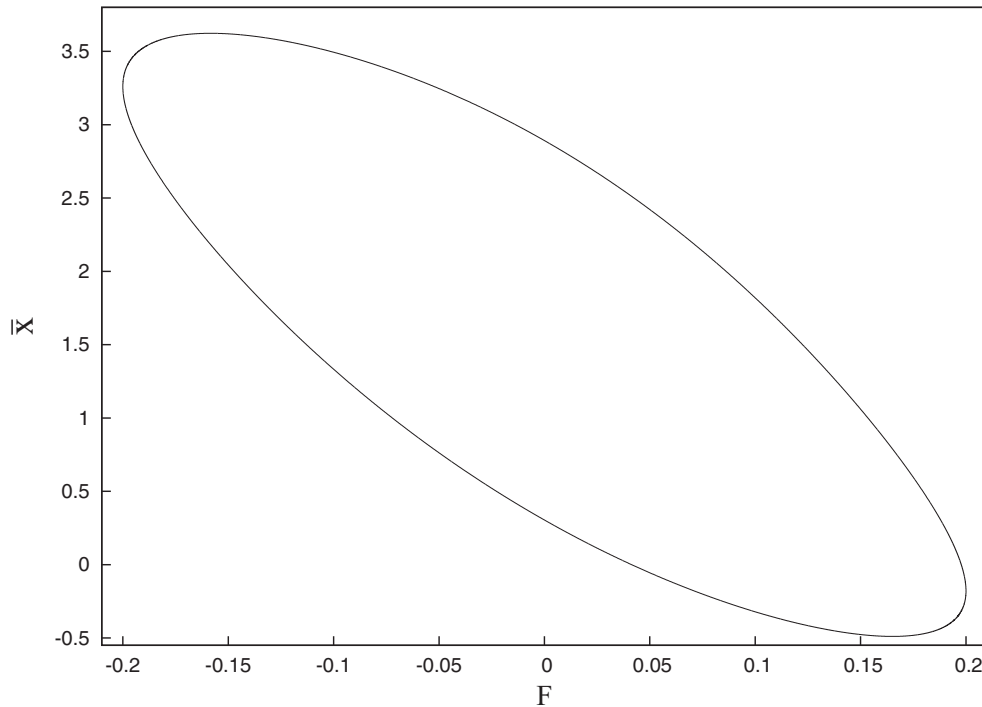

FIG. 1. The mean position $\overline{x}$ as a function of the forcing. Here, $\tau = 8.0$, $\theta = 0.5\pi$, $\gamma_0 = 0.07$, $\lambda = 0.9$, $T = 0.000001$, and $F_0 = 0.2$. This loop represents a large-amplitude state.
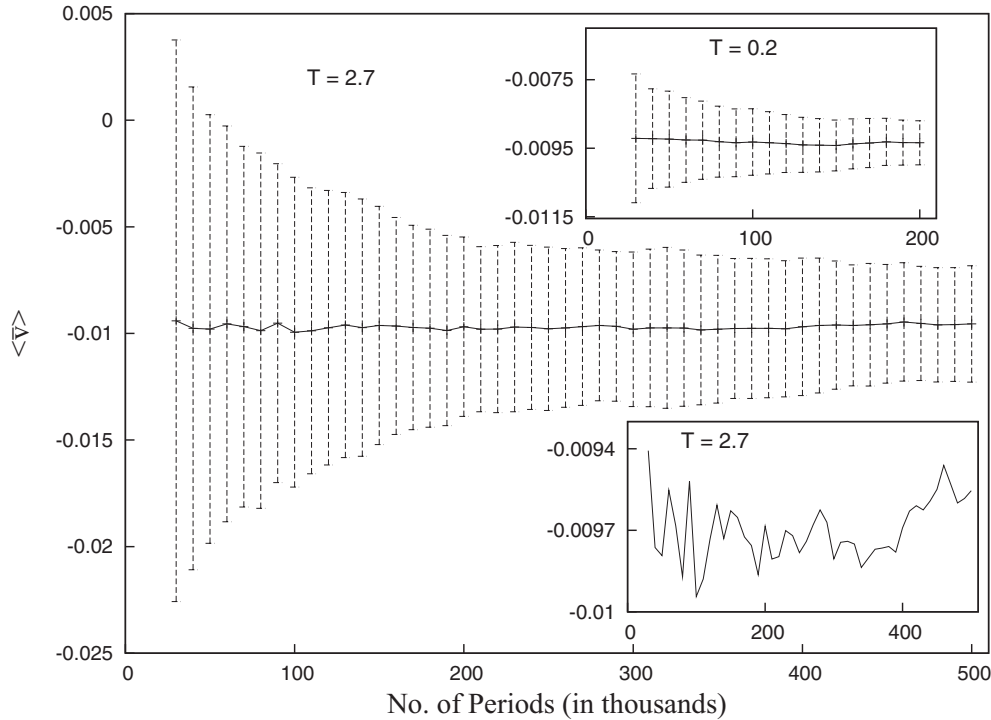
FIG. 2. The mean velocity $\langle \overline{v} \rangle$ as a function of the number of periods of the forcing used to calculate $\overline{v}$'s. The data for $\langle \overline{v} \rangle$ had been recorded for every 10 000 cycles and the corresponding error bars are calculated. Here $\tau = 7.7$, $\theta = 0.5\pi$, $\gamma_0 = 0.07$, $\lambda = 0.9$, $T = 2.7$, and $F_0 = 0.2$. The inset in the bottom-right shows the change of $\langle \overline{v} \rangle$ without error bars. The inset in the top-right corner is same as the main graph but for $T = 0.2$. (Note: The labels on the axes of the insets are same as those of the main graph.)

one trajectory, is calculated as

$$\overline{v} = \frac{1}{N\tau} x(t = N\tau), \qquad (3.4)$$

and the overall mean (net) velocity or the ratchet current, $\langle \overline{v} \rangle$, is calculated as the ensemble average over all the n trajectories. Typically, as discussed below, $N = 200\,000$ for small temperatures and $N = 500\,000$ for large temperatures. The value of N is chosen to have relatively small error bars so the qualitative features of the results (see below) are not obscured.

The error bars are calculated assuming the numerical procedure adopted to be correct and errors occurring only due inherently to the stochastic dynamics of the system. We calculate the $x(N\tau)$ for each initial condition used to calculate $\overline{v} = \frac{x(N\tau)}{N\tau}$. The deviations of these $\overline{v}$ from the mean $\langle \overline{v} \rangle$ calculated as an ensemble average over all trajectories with distinct initial conditions. The standard deviations Δv form the error bars.

At large temperatures the effect of frictional inhomogeneity gets manifest. However, one needs to calculate the mean values carefully. The frictional inhomogeneity provides only a weak (left-right) asymmetry. As a consequence, the ratchet current $\langle \overline{v} \rangle$ obtained is not large and the standard deviations, Δv (error bars), are not small, although they are smaller than the mean $\langle \overline{v} \rangle$. This is especially true when the temperatures are large. Therefore, whereas for smaller temperatures $T < 0.5$ one gets sensible $\langle \overline{v} \rangle$ values, say, $\frac{\Delta v}{\langle \overline{v} \rangle} < 0.2$, when averaged over 200 000 periods of the drive, it takes 500 000 periods at

temperatures $T > 1.0$ to obtain similar sensible $\langle \overline{v} \rangle$ values. Figures 2 and 3 illustrate the above statement succinctly.

In Fig. 3 is also plotted $\frac{2\pi \Delta N}{N\tau}$ as a function of temperature. Here ΔN is the difference between the number of transitions to the left and right direction potential wells and N is the total number of periods of $F(t)$ used to obtain ΔN. The figure shows that $\langle \overline{v} \rangle$ and $\frac{2\pi \Delta N}{N\tau}$ almost coincide. Note that the possibility of the particle making a transition to a potential well farther than the adjacent well of the starting well before getting trapped is not ruled out, although such events are rare at lower temperatures but not so rare at higher temperatures. (These events are actually observed in the trajectory plots.) This naturally brings in the question of distribution of jump lengths (in terms of number of wells) on either directions and hence the dependence of net displacements (and ratchet currents) on the distributions. However, from the matching of $\langle \overline{v} \rangle$ and $\frac{2\pi \Delta N}{N\tau}$ in Fig. 3, we see that the distribution is sharply peaked at the jump length of 2π, or one well length, on either direction; distributions are almost identical on both the directions. Of course, a finite small tail of the distributions corresponding to larger lengths, at least at higher temperatures, is always there.

Of course, clearly, the quantities of our interest $\langle \overline{W} \rangle$ and $\langle \overline{v} \rangle$ depend on the parameters F_0 and $\omega = \frac{2\pi}{\tau}$ of the external field $F(t)$. In what follows we shall keep the amplitude F_0 fixed and equal to 0.2 throughout. The chosen value of F_0 is not only because it corresponds to a subthreshold forcing but it is in a range where one is expected to get desired sensible results [16].
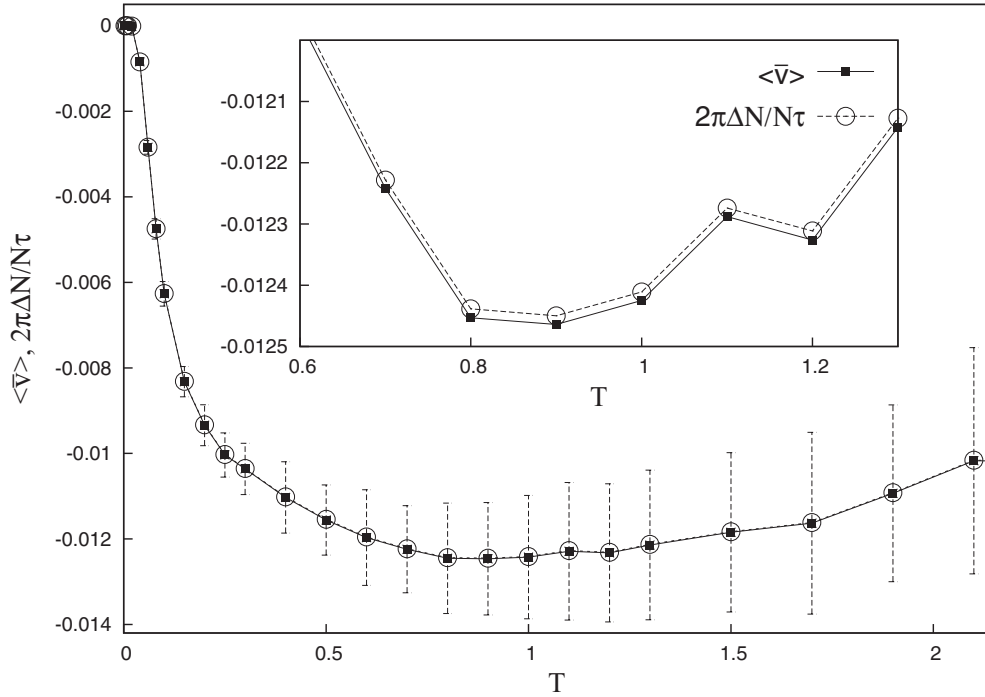
FIG. 3. The mean velocity $\langle \overline{v} \rangle$ as a function of T is shown (dark squares with error bars) for $\tau = 7.7$, $\theta = 0.5\pi$, $\gamma_0 = 0.07$, $\lambda = 0.9$, and $F_0 = 0.2$. In the graph are also included the plot (open circles) of $\frac{2\pi \Delta N}{N\tau}$, where ΔN is the difference between the number of left and right interwell hoppings, and N is the corresponding total number of periods of $F(t)$ considered. The inset shows the magnified image of the main plot (without the error bars) for a limited range of T values, showing that both the quantities $\langle \overline{v} \rangle$ and $\frac{2\pi \Delta N}{N\tau}$ are very close but not exactly equal.

A. Dynamical states of trajectories at low temperatures

Before we begin presenting the numerical results at finite temperatures, we examine the trajectories at a temperature close to zero ($T = 0.000\,001$) as a response to an external field $F(t)$. The nonuniformity of the friction coefficient $\gamma(x) = \gamma_0[1 - \lambda \sin(x + \theta)]$ is measured by the value of λ and its phase shift with respect to $V(x) = -\sin(x)$ by θ. Figure 4 shows typical trajectories in the two states of large amplitude and small amplitude depending on the initial conditions chosen but for the same $F(t)$. These trajectories are periodic as $F(t)$ and are characterized by amplitude x_0 and phase lag [with respect to $F(t)$] ϕ. Since the dynamics are stochastic, the amplitude and phase lag are not the same in every period of

$F(T)$, and only their average values make sense. We measure them in one of two ways: (i) We calculate the mean values of the quantities over several periods from the trajectories or (ii) we calculate from the mean hysteresis loops, Fig. 1, considering this approximately to be an ellipse. However, the second method becomes impractical when the hysteresis loop becomes nonelliptic and in that case the first method is the only option.

In Fig. 5, the variation of x_0 is shown as a function of λ for various values of θ in the two states: the LA state [Fig. 5(a)] and the SA state [Fig. 5(b)]. The percentages of variations are calculated with reference to values at $\lambda = 0$. In Figs. 5(c) and 5(d), the variations of ϕ are shown. It is to be noted, from the
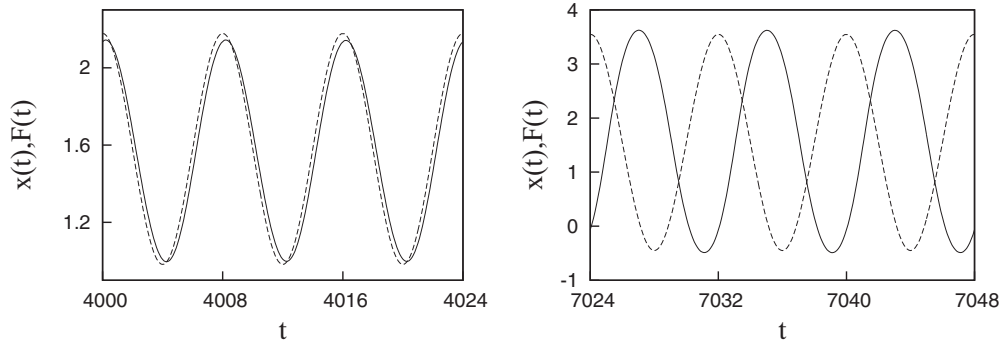

FIG. 4. The figure shows the two dynamical states of trajectories: the SA state (left), with $x(0) = 0.40\pi$, and the LA state (right), with $x(0) = -0.35\pi$, occurring when driven by a cosinusoid of the same amplitude $F_0 = 0.2$ at $T = 0.000\,001$, with $\lambda = 0.9$, $\gamma_0 = 0.08$, $\theta = 0.50\pi$, and $\tau = 8.0$. For both of the figures, the dashed lines represent $F(t)$ multiplied by 2.99 centered at 1.58 and by 10 centered at 1.55, respectively, for easy comparison.
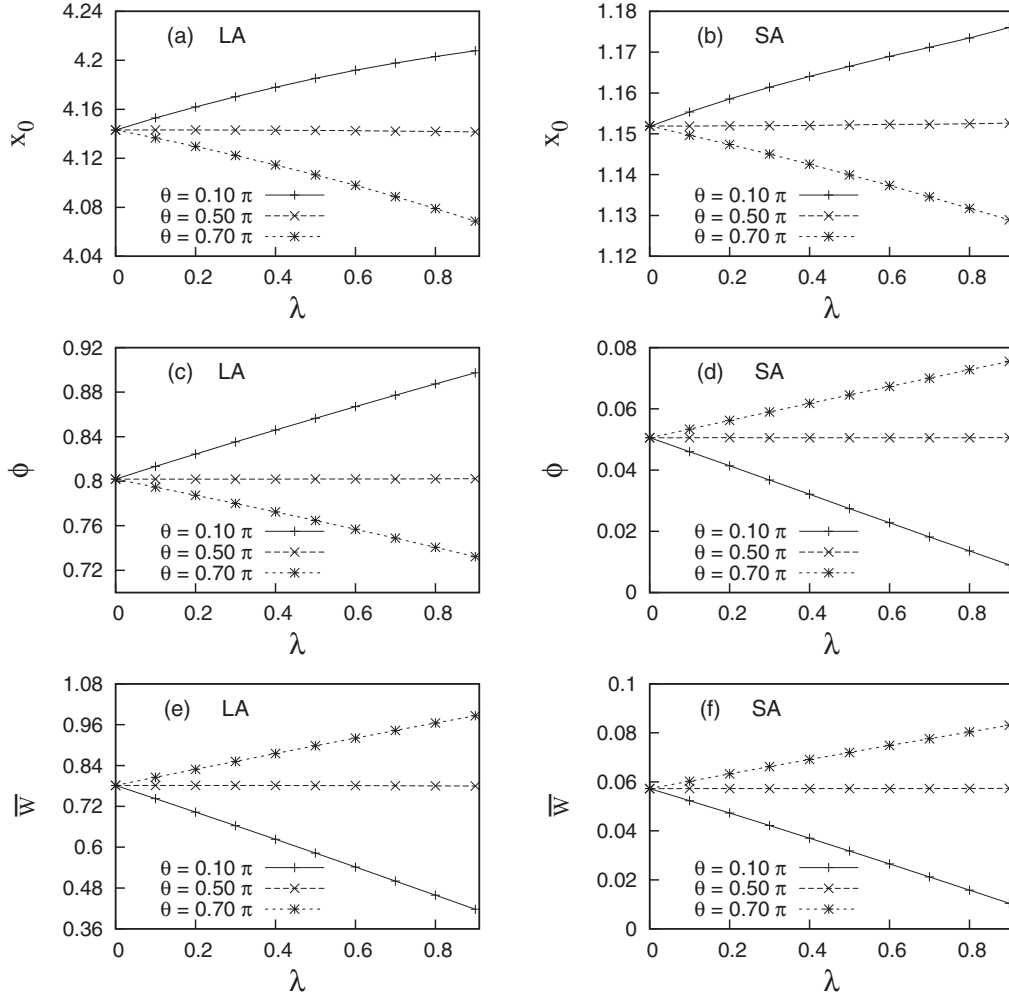
FIG. 5. The changes of x_0, ϕ and $\overline{W}$ with λ for both LA and SA states with $F_0 = 0.2$, $\tau = 8.0$, $\gamma_0 = 0.07$ at $T = 0.000\,001$ and various values of θ as indicated.

figures, that for $\theta = \frac{\pi}{2}$ both x_0 and ϕ almost remain constant (variation less than 0.03%) over the entire range of $0 < \lambda < 1$. For $\theta < \frac{\pi}{2}$, x_0 increases as a function of λ, whereas for $\theta > \frac{\pi}{2}$, x_0 decreases with an increase of λ for both the LA and SA states. However, these variations are very small, less than 2% at $\lambda = 0.9$. In the SA state the values of ϕ themselves are very small and hence their variations, though very small, appear to be large in percentage. In this state, for $\theta < \frac{\pi}{2}$, ϕ decreases and for $\theta > \frac{\pi}{2}$, it increases as a function of λ. The LA state has large values of ϕ, for example, $\phi \sim 0.8\pi$ at $\theta = \frac{\pi}{2}$. In this LA state, as λ is increased from a small value ($\lambda \approx 0$) to a large value, ϕ increases for $\theta < \frac{\pi}{2}$, whereas it decreases for $\theta > \frac{\pi}{2}$. These variations are comparatively large ($\leqslant 10\%$). Since the variations of x_0 are small the variations of the hysteresis $\overline{[x(F)]}$ loop area $\overline{A}$ (or the input energy $\overline{W}$) in the two states are determined essentially by the variations of ϕ. Note that $\phi = \frac{\pi}{2}$ should have the largest $\overline{W}$ for a given x_0. These varations of $\overline{W}$ are shown in Figs. 5(e) and 5(f).

In what follows we shall keep the value of $\lambda = 0.9$ fixed. For $\lambda = 0.9$ the results of Figs. 5 are summarized in Figs. 6(a)–6(f): $x_0(\theta)$, $\phi(\theta)$, and $\overline{W}(\theta)$ for both the LA and SA states. Again, the variation of $\overline{W}(\theta)$ is determined by the variation of $\phi(\theta)$; for the LA state ϕ decreases towards $\frac{\pi}{2}$ (and hence $\overline{W}$ increases),

whereas for the SA state ϕ increases as θ is increased (again thereby increasing $\overline{W}$). Note that, since the particle moves in a periodic potential with a potential barrier of magnitude 2, whereas the drive amplitude is only 0.2 (and hence the maximum reduction in potential barrier $= 0.4\pi$), the particle will remain confined to the same well of the potential at low temperatures. Only when the temperature is increased will the particle have any chance of overcoming the potential barrier. Therefore, the mean net velocity $\langle \overline{v} \rangle$ is zero at low temperatures even though $\langle \overline{W} \rangle$ is nonzero at all temperatures.

Figure 7 shows the coexistence boundary of the two dynamical states in the (γ_0, τ) space for $\theta = 0.25\pi, 0.5\pi$, and 0.75π. In the inset of the figure are shown the loci of various fractions of the SA state within the coexistence boundary for $\theta = 0.5\pi$. Similar loci for other values of θ have also been calculated but are not shown here. However, the consequences of such fractions at any point in the (γ_0, τ) space will be discussed later. Clearly, the upper limit of γ_0 for the coexistence region decreases as θ increases. This behavior of θ dependence can be understood if the relationship between the potential $V(x)$ and $\gamma(x)$ is examined. It will be easier to visualize if a rectangular profile of $\gamma(x)$ is considered, for illustration, instead of a sinusoidal profile. This is justified because it has
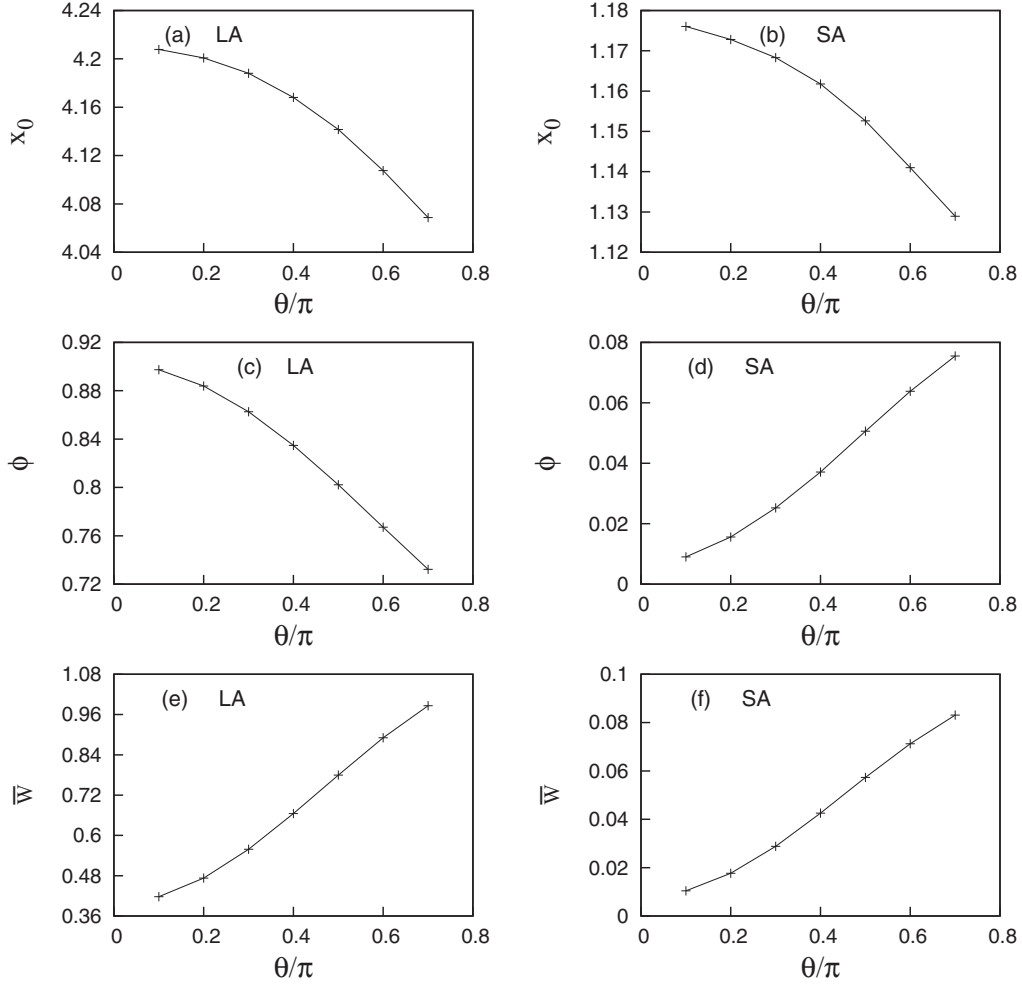
FIG. 6. The changes of x_0, ϕ, and $\overline{W}$ with θ for both the LA and SA states with $F_0 = 0.2$, $\tau = 8.0$, $\gamma_0 = 0.07$ at $T = 0.000\,001$, keeping $\lambda = 0.9$ fixed.

been found that rectangular and sinusoidal profiles of $\gamma(x)$ yield essentially similar transport characteristics.

In Fig. 8, as an illustration, the potential $V(x)$ and rectangular $\gamma(x)$ are plotted together for the phase difference $\theta = 0.5\pi$ (a) and $\theta = 0.25\pi$ (b). Since $V(x)$, is sinusoidal the space between two consecutive minima forms a period. From Fig. 8(a) one can see that $\gamma(x)$ is large over the entire half period to the left of $V(x)$ peak, whereas $\gamma(x)$ is small over the rest half period, to the right, of $V(x)$ peak. Therefore, a particle will experience a moderate effective damping force, of magnitude, say, F_{eff}, measured roughly by the averaged product $\gamma(x)v(x(t))$ over a period. On the other hand, from Fig. 8(b), for $\theta = 0.25\pi$, one can see that at the bottom of the potential, where the particle velocity is expected to be large, the friction coefficient γ is small and at the peak of the potential, where the velocity should be small the friction is large. Thus, one can conclude that the effective damping force experienced by the particle in this case will be smaller than F_{eff} of the former case and hence the particle will be more mobile in this case of smaller θ. From a similar consideration one can see that the effective damping force experienced by the particle in the case of, say, $\theta = 0.75\pi$ will be larger than F_{eff}. In other words, the average mobility of the particle decreases as

a function of θ for the same forcing and the potential function. Though difficult to define, one can think of a uniform effective friction coefficient $\overline{\gamma_0}$ for each θ [for nonuniform $\gamma(x)$] for a given potential function and external field, as in case of Ref. [15]. Thus, one can argue that the average effective friction coefficient, $\overline{\gamma_0}$, increases monotonically as θ is changed from 0 to π in $\gamma(x) = \gamma_0[1 - \lambda \sin(x + \theta)]$. This explains why the (γ_0, τ) region of coexistence of the two dynamical states in Fig. 7 shrinks as θ increases in order to have the same effective γ at the upper coexistence limit.

B. Ratchet current and input energy at finite temperatures

From the above analysis one can conclude that for a given pair of (γ_0, τ) values the effective friction coefficient $\overline{\gamma_0}$ increases with θ and, hence, as can be seen in Fig. 9, the total number (N_t) of interwell transitions at a given temperature T decreases monotonically. This, however, does in no way imply that the ratchet current decreases monotonically with increasing θ.

As can be seen, in Fig. 10, the ratchet current, which is also a measure of difference between the interwell transitions in the right and left directions, peaks around $\theta = 0.5\pi$.
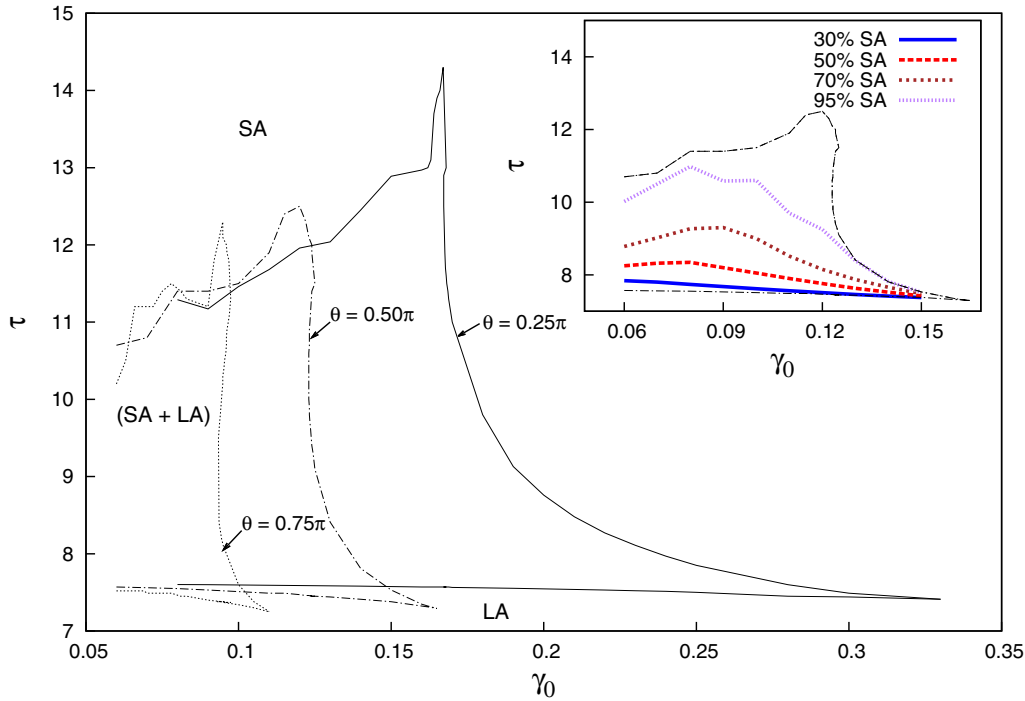
FIG. 7. The figure shows the boundaries of regions of coexistence of the SA and LA states for $\theta = 0.25\pi, 0.5\pi$, and 0.75π at $T = 0.000\,001$. Observe that $\theta = 0.25\pi$ provides a larger maximum limiting value of γ_0 in the (τ, γ_0) space for the coexistence of the dynamical states. Clearly, with $\theta = 0.75\pi$, the limiting value of γ_0 has reduced significantly. In the inset are shown the loci of various percentages of populations of the SA state for $\theta = 0.5\pi$ at $T = 0.000\,001$.

Since $\theta = 0.5\pi$ provides the largest frictional asymmetry one would ideally think of the ratchet current to be maximum at $\theta = 0.5\pi$. However, at lower temperatures the ratchet current actually peaks at $\theta < 0.5\pi$, Fig. 10. This is because lower θ corresponds to lower effective $\overline{\gamma_0}$ and hence, being more mobile, interwell transitions begin at lower temperatures than for larger θ. Thus ratchet current grows faster, beginning at lower temperatures, for smaller θ and hence dominates before the frictional asymmetry overwhelms it at larger temperatures, where one can find the ratchet current to be the maximum for $\theta = 0.5\pi$, inset of Fig. 10.

In Fig. 11, the input energy $\langle \overline{W} \rangle$ is plotted as a function of θ for two temperatures, (i) $T = 0.000\,001$, based on the weightage average of results for the LA and SA states

[Figs. 6(e) and 6(f)], and (ii) $T = 0.2$, for $\gamma_0 = 0.07$ and $\tau = 7.7$. At low temperatures, $\langle \overline{W} \rangle(\theta)$ strongly depends on the choice of the point (γ_0, τ) and the variation can be explained with the help of the coexistence diagrams (Fig. 7) and the loci of fractions of the SA states. The inset of Fig. 11 shows some representative loci of the fractions of the SA state for $\theta = 0.25\pi, 0.5\pi$, and 0.75π together around the point $(0.07, 7.7)$ in the (γ_0, τ) space. One can find that the fractions of the SA states for $\theta = 0.75\pi$ is 38.5%, for $\theta = 0.5\pi$ it is 25%, and for $\theta = 0.25\pi$ it is 17.5%. In other words, the fractions of the LA states are, respectively, 61.5%, 75%, and 82.5% for $\theta = 0.75\pi, 0.5\pi$, and 0.25π. Since $\overline{W}$ for LA states are much larger compared to $\overline{W}$ for SA states, the weightage average $\langle \overline{W} \rangle$ decreases with θ because the fraction of LA states
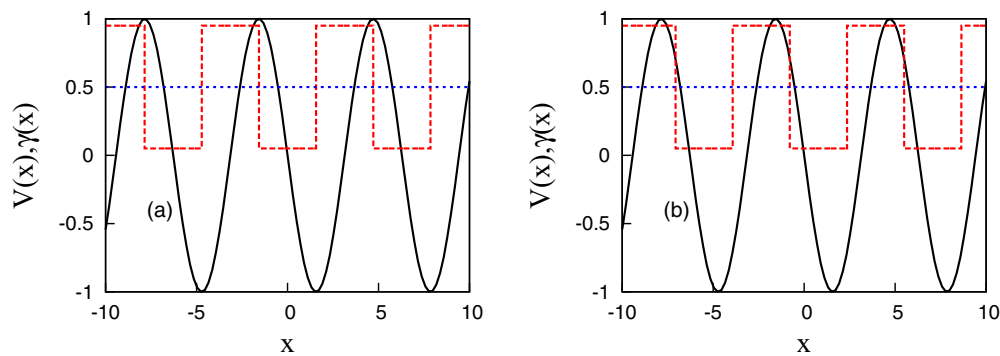

FIG. 8. The above two figures compare the the potential $V(x)$ (black) and the (square-wave type) friction coefficient $\gamma(x)$ (red). The left figure is for $\theta = 0.50\pi$ and the right figure is for $\theta = 0.25\pi$. The blue line in both figures is the mean value of $\gamma(x)$, here taken as $\gamma_0 = 0.5$ for better comparison.
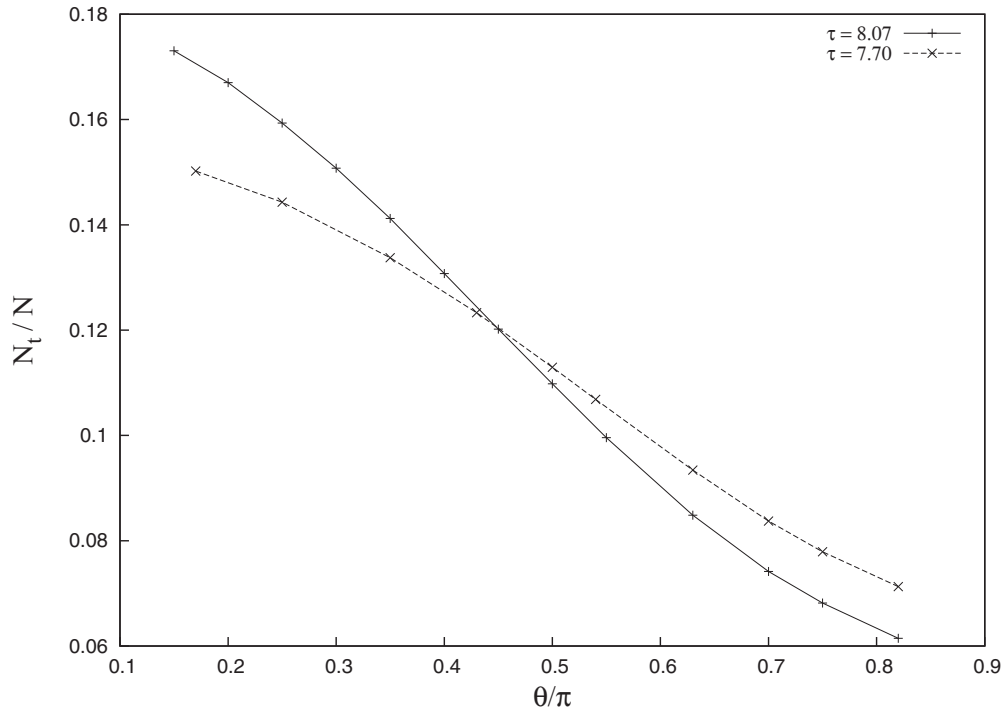
FIG. 9. The figure shows the decrease of the fraction of the total number of interwell hoppings ($\frac{N_t}{N}$) as a function of θ for two τ values, $\tau = 8.07$ (upper plot) and $\tau = 7.70$ (bottom plot) in 200 000 periods of $F(t)$. Here $T = 0.2$, $F_0 = 0.2$, $\gamma_0 = 0.07$, and $\lambda = 0.9$.

decreases with θ. However, the $\overline{W}$ for the LA and SA states are monotonically increasing as a function of θ (Fig. 6), implying thereby that $\langle \overline{W} \rangle$ increases with θ if the fractions are kept fixed. These two opposing trends of variations of $\langle \overline{W} \rangle$ as a function of θ leads to the peaking behavior of $\langle \overline{W} \rangle$ as a function of θ

at low temperatures. However, as the temperature is increased the transitions between the LA and SA states allow the SA states to appear where previously only LA states existed and vice versa. This makes the coexistence boundaries of Fig. 7 blurred and nonexistent and hence $\langle \overline{W} \rangle(\theta)$ gets smoothened.
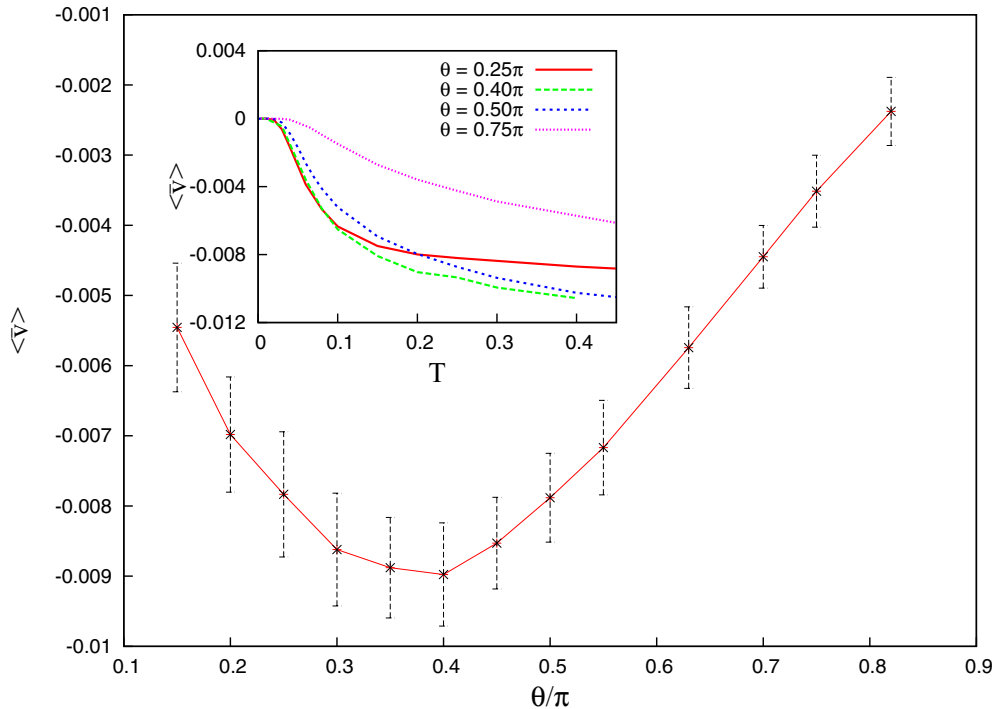

FIG. 10. The change of mean velocity $\langle \overline{v} \rangle$ with θ at $T = 0.2$ for $\tau = 8.07$, $\lambda = 0.9$, and $F_0 = 0.2$. The inset shows the change of $\langle \overline{v} \rangle$ with T for $\tau = 8.07$ but for different θ values, as indicated in the plot, keeping other parameters same.
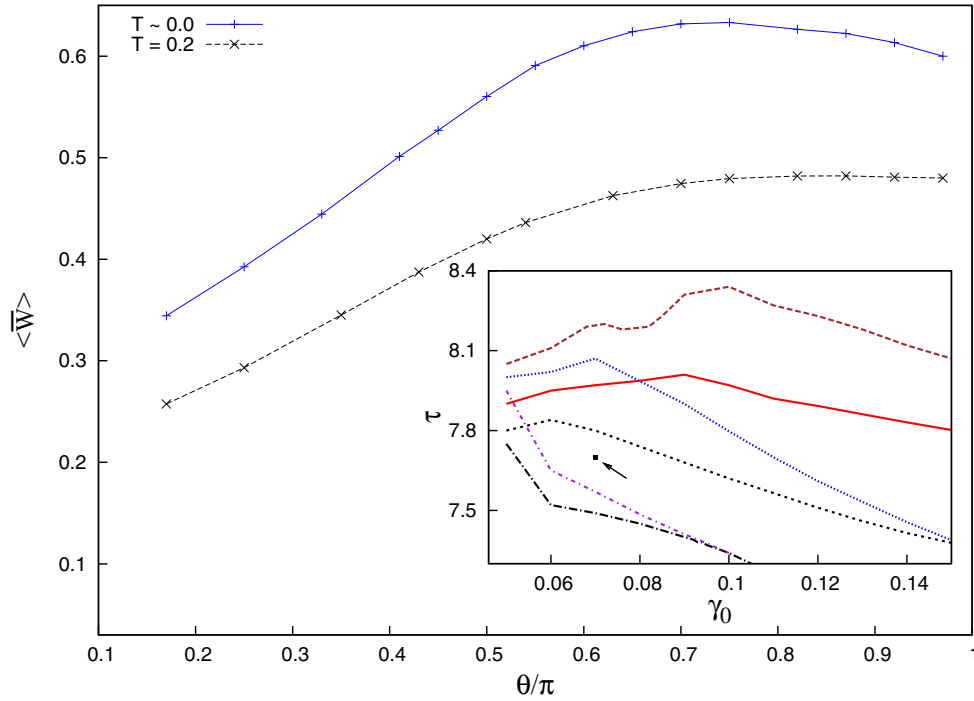
FIG. 11. The mean energy $\langle \overline{W} \rangle$ as a function of θ is shown for $\tau = 7.70$, $F_0 = 0.2$, $\lambda = 0.9$, $\gamma_0 = 0.07$ at $T = 0.000001$ (blue) and $T = 0.2$ (black). The inset shows the loci of constant percentages of population of the SA state in the (τ-γ) space at $T = 0.000001$ for various θ values: 30% population of SA states when $\theta = 0.25\pi$, $\theta = 0.50\pi$, and $\theta = 0.75\pi$ are, respectively, depicted by red, black dotted, and black dash-dotted lines, whereas a 40% population of SA states are correspondingly shown in brown, blue, and purple. The point ($\gamma_0 = 0.07, \tau = 7.7$) is marked in the inset.
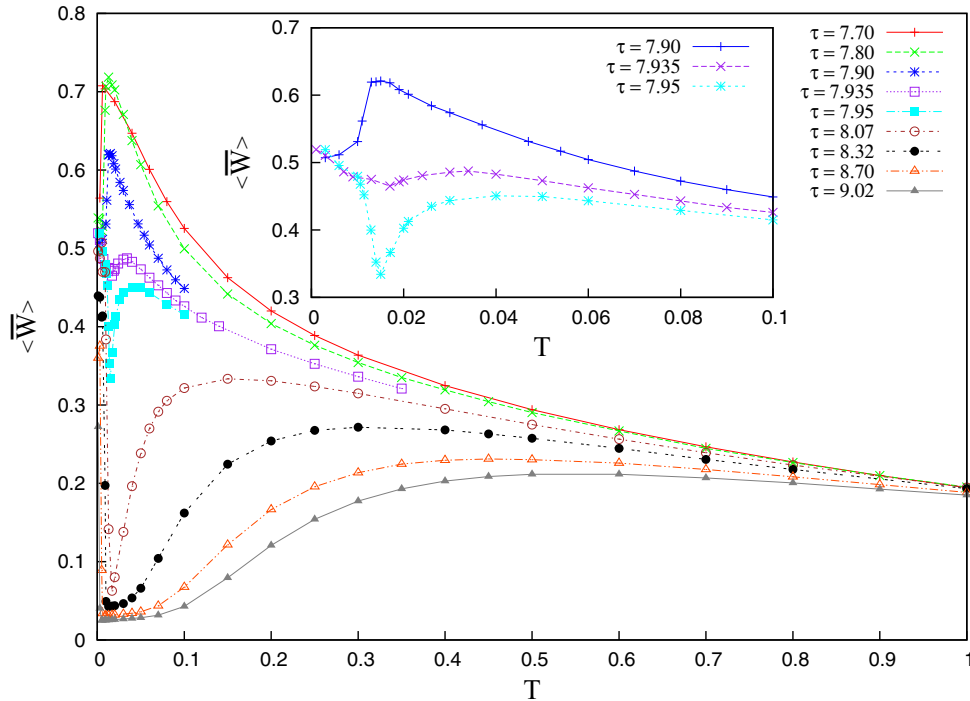

FIG. 12. The mean energy $\langle \overline{W} \rangle$ as a function of T for various τ values as indicated in the top-right corner of the figure with $F_0 = 0.2$, $\gamma_0 = 0.07$, $\lambda = 0.9$, $\theta = 0.50\pi$. The inset displays the two differing nature of input energy variations at low temperatures with $\tau \approx 7.935$ as the boundary.
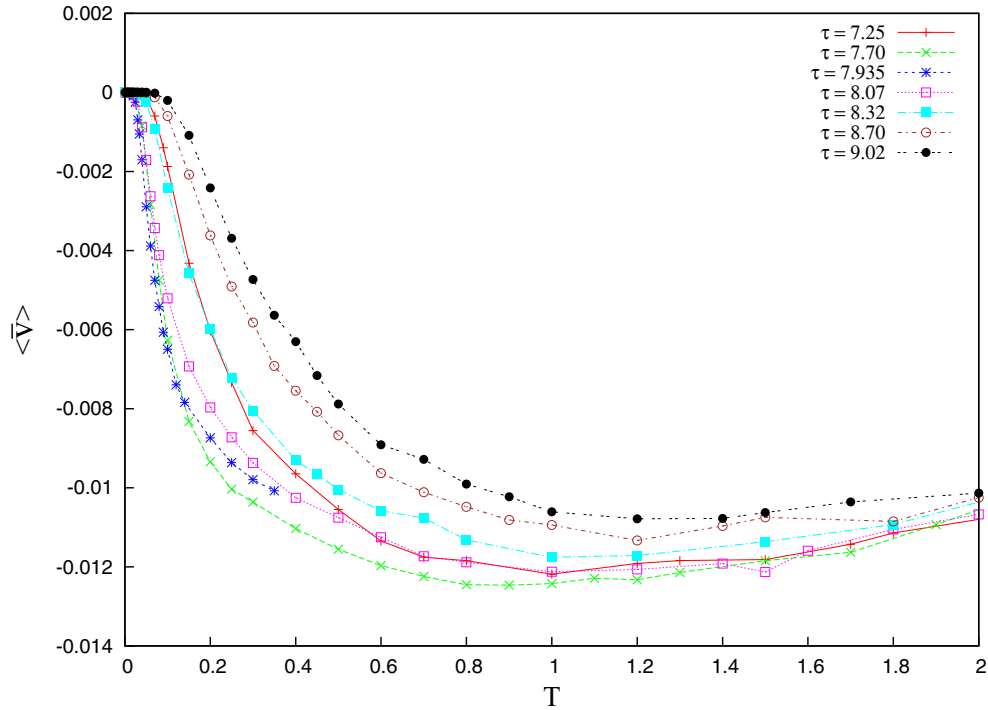
FIG. 13. The mean velocity $\langle \overline{v} \rangle$ as a function of T for various τ values as indicated in the top-right corner of the figure with $F_0 = 0.2$, $\gamma_0 = 0.07$, $\lambda = 0.9$, $\theta = 0.50\pi$.

Figure 11(b) shows that, at $T = 0.2$, $\langle \overline{W} \rangle(\theta)$ is monotonic, which is to be compared with $\langle \overline{v} \rangle$, shown in Fig. 10, showing a peak close to $\theta = \frac{\pi}{2}$ irrespective of the choice of (γ_0, τ) point. Thus, there is no correlation between energy absorption and the ratchet current, at least as far as variation with respect to θ is concerned.

Figure 7 also provides a guideline to choose the region of (γ_0, τ) space in order to obtain stochastic resonance for a given
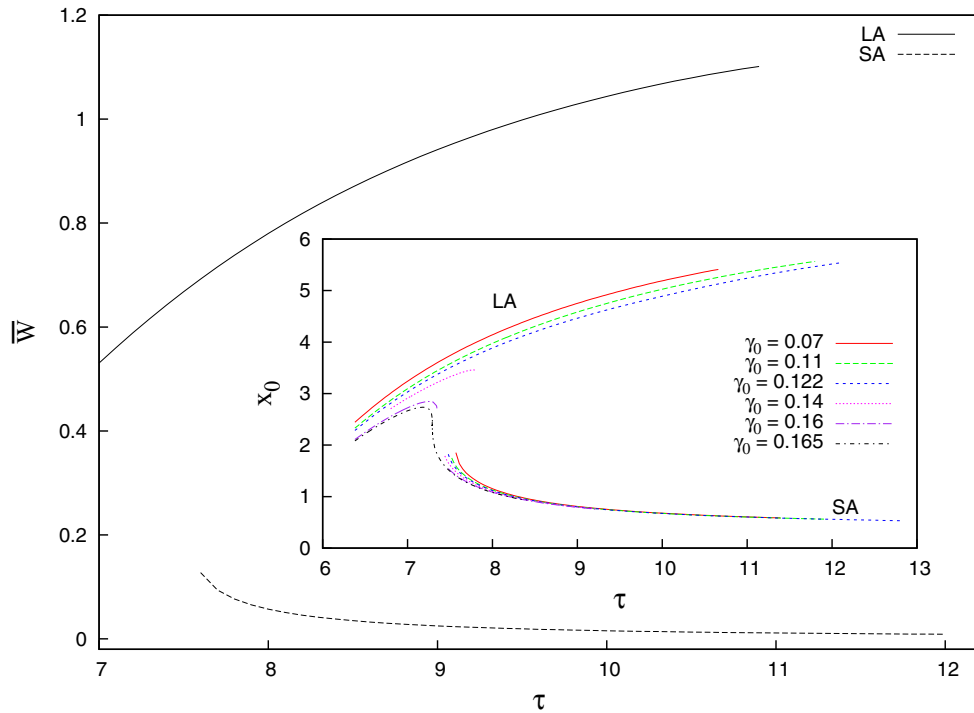

FIG. 14. The mean energy $\overline{W}$ as a function of τ at $T = 0.000\,001$ for the two dynamical (LA and SA) states as indicated, with $F_0 = 0.2$, $\gamma_0 = 0.07$, $\lambda = 0.9$, $\theta = 0.50\pi$. The inset shows the change of amplitude x_0 as a function of τ for both LA and SA states at $T = 0.000\,001$, $\lambda = 0.9$, $F_0 = 0.2$, $\theta = 0.5\pi$ for different γ_0 values as indicated.
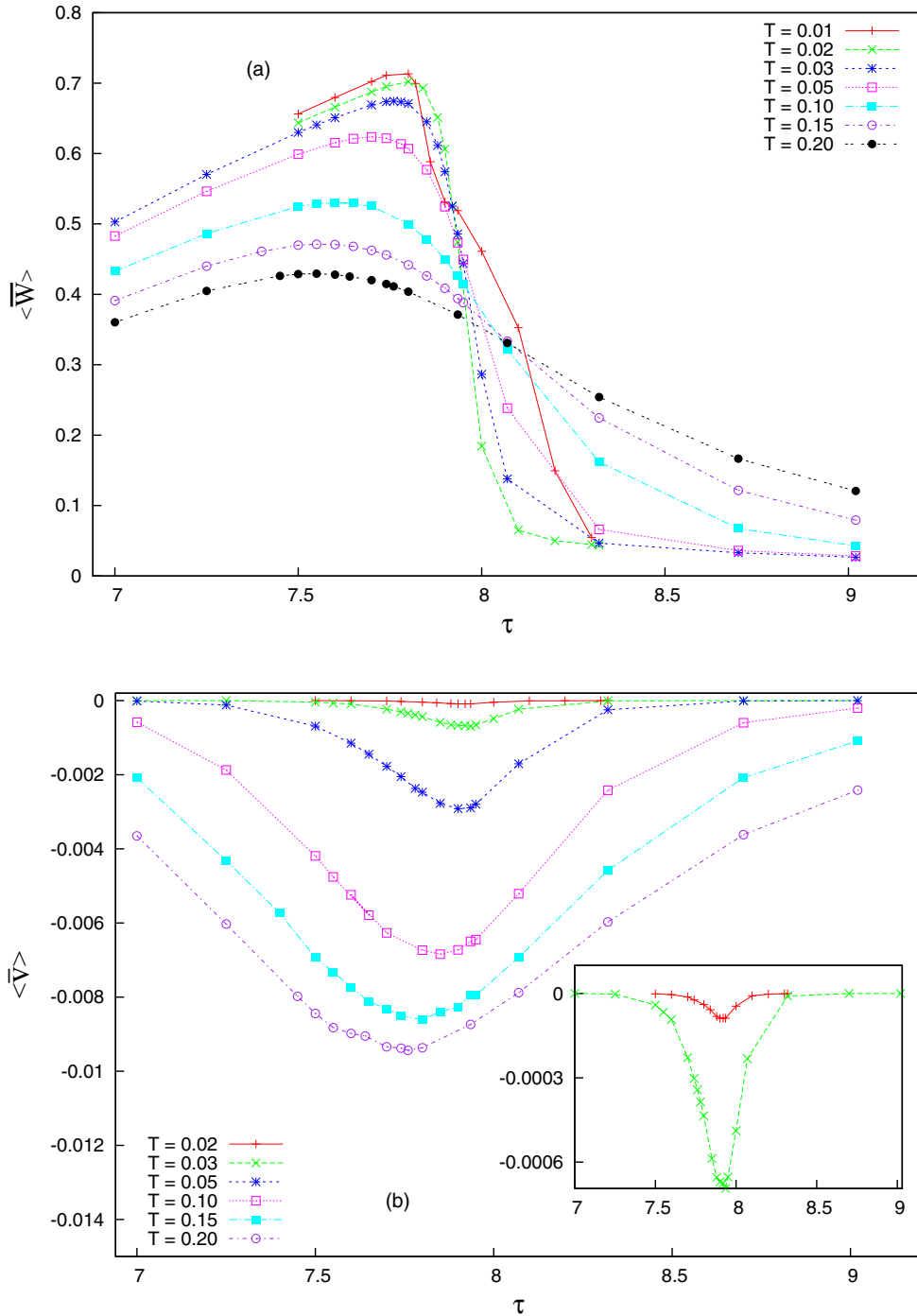
FIG. 15. The change of $\langle \overline{W} \rangle$ with τ is shown in Fig. 15(a) and that of $\langle \overline{v} \rangle$ in Fig. 15(b) for various small temperatures as indicated, with $F_0 = 0.2$, $\gamma_0 = 0.07$, $\lambda = 0.9$, $\theta = 0.50\pi$. The inset in Fig. 15(b), with the same axes label as the main plot, shows the two curves for lower temperatures $T = 0.02$ and $T = 0.03$ for clarity.

θ. Invariably, stochastic resonance occurs if the region of (γ_0, τ) space is chosen such that both the dynamical states coexist, at low temperatures (for example, $T = 0.000\,001$), with their fractions not too far away from 0.5. In Fig. 12, the mean energy absorbed $\langle \overline{W} \rangle$ is plotted against temperature for various values of τ with $\gamma_0 = 0.07$. In Fig. 13, the ratchet current $\langle \overline{v} \rangle$ is plotted for the same parameters. From these figures one can observe that stochastic resonance and ratchet effect do occur simultaneously in the same parameter space. Note, however,

that the temperatures at which $\langle \overline{W} \rangle$ and $\langle \overline{v} \rangle$ peak are widely separated; stochastic resonance and peak of ratchet current do not occur at nearby temperatures. Similar results were also obtained earlier when a homogeneous system was driven by a biharmonic forcing [26]. Figures 12 and 13, obtained for an inhomogeneous system driven by a sinusoidal field, are the main results of the present work and deserve further analysis.

Figure 14 shows the variation of the input energy (or energy absorbed) per cycle, $\overline{W}$, of $F(t)$ as a function of the period τ
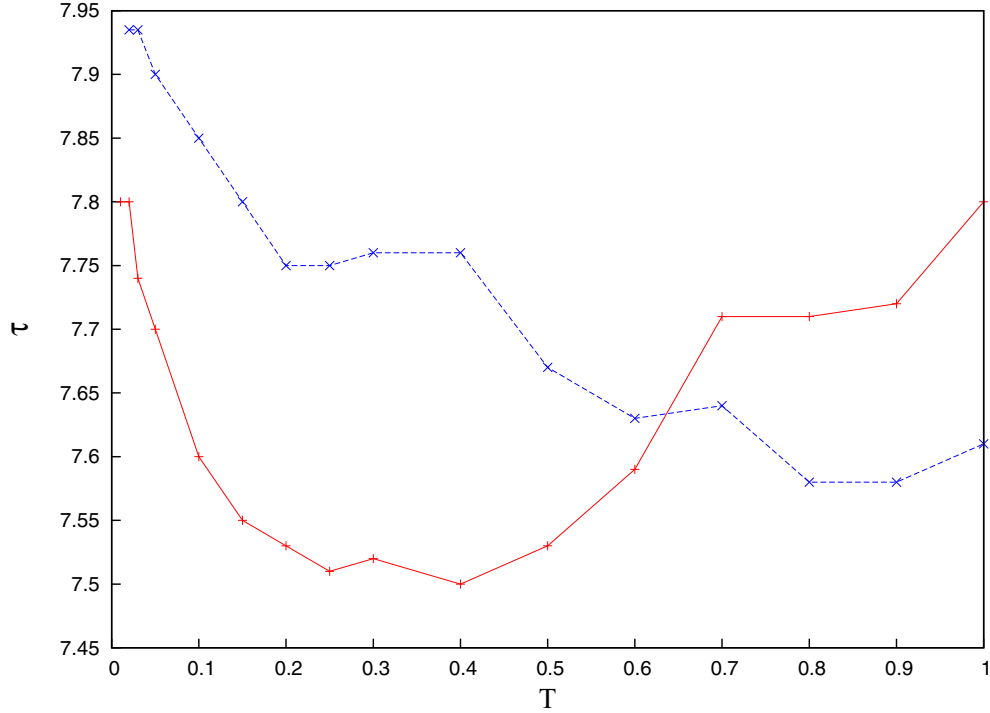
FIG. 16. The figure records the τ values corresponding to maximum $\langle \overline{W} \rangle$ (in red) and maximum $\langle \overline{v} \rangle$ (in blue) as T is changed, with $F_0 = 0.2$, $\gamma_0 = 0.07$, $\lambda = 0.9$, $\theta = 0.50\pi$.

of $F(t)$ in the LA and SA states at very low temperatures $T \approx 0$ and $\gamma_0 = 0.07$. Of course, the comparison makes sense only in the coexistence region of (γ_0, τ) space. The trend of variation of $\overline{W}$ qualitatively follows that of the amplitude x_0 of the trajectories, as indicated by the curves in the inset of the figure. The trend remains the same as the temperature is increased by a small amount. Note that in the LA state the system absorbs more energy per cycle than when it is in the state SA. Of course, the mean input energy $\langle \overline{W} \rangle$, as discussed earlier, is the weightage average of $\overline{W}$ in the two states. In view of these results and based on the nature of variation of the curves in Fig. 12 at low temperatures, the set of curves in Fig. 12 can be put in two qualitatively distinct groups: one roughly with $\tau \gtrsim 7.935$ and the other with $\tau \lesssim 7.935$, though the dividing line $\tau = 7.935$ is not precise. The decrease of $\langle \overline{W} \rangle$ due to thermal fluctuations as the temperature is raised from $T = 0$ indicates transition from the LA state to the SA state. This shows that for the former group of curves with larger τ the dynamical (SA) state is more stable compared to the LA state. On the other hand, for the latter group of curves with lower τ the LA state is more stable compared to the SA state. This is consistent with the diagram shown in Fig. 7. This is also understandable because the larger the frequency (smaller period) of drive the larger the phase lag should be and hence the LA state (with larger phase lag) should be preferred and vice versa.

IV. DISCUSSION AND CONCLUSION

We presented above the results of our calculations as a function of T and θ for various values of γ_0 and τ. The results are consistent with each other and bear plausible explanations.

However, some detailed results as a function of τ (or frequency, $\frac{2\pi}{\tau}$) need further scrutiny, for which, at present, we lack clear explanation.

In Figs. 15(a) and 15(b) are presented the variations of $\langle \overline{W} \rangle$ and $\langle \overline{v} \rangle$ as a function of τ for $\gamma_0 = 0.07$ and $\theta = 0.5\pi$ at various temperatures. Particular attention may be given to the occurrence of maxima of $\langle \overline{W} \rangle$ and $\langle \overline{v} \rangle$ at low temperatures as summarized in Fig. 16.

From Fig. 14, it is clear that $\overline{W}$ for LA states is much larger than for the SA states, and one would, therefore, expect $\langle \overline{W} \rangle$ to peak just before the SA states make their appearance around $\tau = 7.5$, unless the loss due to the appearance of the SA states is more than compensated for by the rise of $\overline{W}$ with increase in τ. However, the slope of $\overline{W}(\tau)$ is not so large as to offset the loss due to the appearance of the SA states, yet $\langle \overline{W} \rangle$ peaks at a value of τ larger than 7.5. Though this anomaly is curious, the peaking of $\langle \overline{v} \rangle$ at low temperatures is more interesting. $\langle \overline{v} \rangle$ peaks at a value of $\tau \sim 7.935$ where the SA and LA states are nearly equally stable. (As concluded earlier, at smaller τ the LA state is more stable than the SA state and vice versa.) In other words, at low temperatures, the asymmetry in the probability of crossings to the left and right wells of the periodic potential become the largest at that value τ for which the LA and SA states are equally stable.

Although $\langle \overline{W} \rangle$ and $\langle \overline{v} \rangle$ do not peak at the same τ values, the difference in τ values at which they peak is much smaller compared to the range of τ over which the two states coexist. However, for given values of γ_0 and τ, $\langle \overline{W} \rangle$ and $\langle \overline{v} \rangle$ peak at widely separated temperatures, Fig. 16. Thus the variation of $\langle \overline{W} \rangle$ and $\langle \overline{v} \rangle$ as a function of frequency is nearer to coincidence than the peaking of $\langle \overline{W} \rangle$ (stochastic resonance) and $\langle \overline{v} \rangle$ as a function of temperature.

As stated earlier, frictional inhomogeneity is a comparatively weak agent to yield a ratchet effect, yet the maximum ratchet current that we obtain is not negligible and there is a possibility of obtaining a still-larger current if the parameters are tuned suitably. For example, we have not yet completely explored the variation of $\langle \overline{W} \rangle$ and $\langle \overline{v} \rangle$ as a function of γ_0 which may yield a larger ratchet current.

In summary, we are closer to finding answers to all questions that we had mentioned to begin with. We could observe stochastic resonance and a ratchet effect in the same region of parameter space. However, SR and the ratchet current peak do not occur at the same temperature. We now have a better idea about the relative roles played by the parameters θ and λ characterizing the frictional inhomogeneity and also the periodicity τ of the external periodic field to obtain $\langle \overline{W} \rangle$ and $\langle \overline{v} \rangle$.

ACKNOWLEDGMENTS

[1] H. Risken, *The Fokker-Planck Equation* (Springer-Verlag, Berlin, 1989), Chap. 11.

[2] K. Svoboda, C. F. Schmidt, B. J. Schnapp, and S. M. Block, Nature **365**, 721 (1993); J. T. Finer, R. S. Simmons, and J. A. Spudich, *ibid.* **368**, 113 (1994); D. Jones, *ibid.* **368**, 694 (1994).

[3] P. Reimann, Phys. Rep. **361**, 57 (2002).

[4] M. O. Magnasco, Phys. Rev. Lett. **71**, 1477 (1993); **72**, 2656 (1994).

[5] J. Prost, J. F. Chauwin, L. Peliti, and A. Ajdari, Phys. Rev. Lett. **72**, 2652 (1994); R. D. Astumian and M. Bier, *ibid.* **72**, 1766 (1994).

[6] F. Jülicher, A. Ajdari, and J. Prost, Rev. Mod. Phys. **69**, 1269 (1996).

[7] J. Maddox, Nature **369**, 181 (1994); **369**, 271 (1994).

[8] J. Rousselet, L. Salome, A. Ajdari, and J. Prost, Nature **370**, 446 (1994).

[9] R. Benzi, A. Sutera, and A. Vulpiani, J. Phys. A **14**, L453 (1981).

[10] L. Gammaitoni, P. Hänggi, P. Jung, and F. Marchesoni, Rev. Mod. Phys. **70**, 223 (1998).

[11] T. Wellens, V. Shatokhin, and A. Buchleitner, Rep. Prog. Phys. **67**, 45 (2004).

[12] B. McNamara and K. Wiesenfeld, Phys. Rev. A **39**, 4854 (1989).

[13] S. Fauve and F. Heslot, Phys. Lett. A **97**, 5 (1983).

[14] B. McNamara, K. Wiesenfeld, and R. Roy, Phys. Rev. Lett. **60**, 2626 (1988).

[15] S. Saikia, A. M. Jayannavar, and M. C. Mahato, Phys. Rev. E **83**, 061121 (2011); W. L. Reenbohn, S. S. Pohlong, and M. C. Mahato, *ibid.* **85**, 031144 (2012); S. Saikia, Physica A **46**, 411 (2014)

[16] W. L. Reenbohn and M. C. Mahato, Phys. Rev. E **88**, 032143 (2013).

[17] K. Liu and Y. Jin, Physica A **392**, 5283 (2013).

[18] Y. W. Kim and W. Sung, Phys. Rev. E **57**, R6237 (1998).

[19] M. Büttiker, Z. Phys. B Con. Mat. **68**, 161 (1987).

[20] R. Landauer, J. Stat. Phys. **52**, 233 (1988).

[21] Ya. M. Blanter and M. Büttiker, Phys. Rev. Lett. **81**, 4040 (1998).

[22] R. Benjamin and R. Kawai, Phys. Rev. E **77**, 051132 (2008).

[23] W. L. Reenbohn and M. C. Mahato, J. Stat. Mech.: Theory Exp. (2009) P03011.

[24] D. Dan, M. C. Mahato, and A. M. Jayannavar, Phys. Rev. E **60**, 6421 (1999); D. Dan, A. M. Jayannavar, and M. C. Mahato, Int. J. Mod. Phys. B **14**, 1585 (2000); D. Dan, M. C. Mahato, and A. M. Jayannavar, Physica A **296**, 375 (2001); Phys. Rev. E **63**, 056307 (2001); W. L. Reenbohn, S. Saikia, R. Roy, and M. C. Mahato, Pramana-J. Phys. **71**, 297 (2008).

[25] M. Qian, Y. Wang, and X.-J. Zhang, Chin. Phys. Lett. **20**, 810 (2003).

[26] W. L. Reenbohn and M. C. Mahato, Phys. Rev. E **91**, 052151 (2015).

[27] J. M. Sancho, M. San Miguel, and D. Dürr, J. Stat. Phys. **28**, 291 (1982).

[28] A. M. Jayannavar and M. C. Mahato, Pramana J. Phys. **45**, 369 (1995).

[29] E. A. Desloge, Am. J. Phys. **62**, 601 (1994).

[30] W. H. Press, B. P. Flannery, S. A. Teukolsky, and W. T. Vetterling, *Numerical Recipes* (Cambridge University Press, Cambridge, UK, 1987).

[31] M. C. Mahato and S. R. Shenoy, Phys. Rev. E **50**, 2503 (1994); T. Iwai, Physica A **300**, 350 (2001); M. Evstigneev, P. Reimann, C. Schmitt, and C. Bechinger, J. Phys.: Condens. Matter **17**, S3795 (2005).

[32] R. Mannella, A gentle introduction to the integration of stochastic differential equations, in *Stochastic Processes in Physics, Chemistry, and Biology*, edited by J. A. Freund and T. Pöschel, Lecture Notes in Physics Vol. 557 (Springer, Berlin, 2000), p. 353.

[33] K. Sekimoto, J. Phys. Soc. Jpn. **66**, 1234 (1997).